International Journal of Nanoelectronics and Materials
Volume 12, No. 2, Apr 2019 [123-134]

Effect of Deposition Direction on the Properties of Silicon layers Fabricated from Recycled Silicon Powder

Alaa A. Abdul-Hamead*

Materials Engineering Department / University of Technology, Baghdad- Iraq.

Received 11 June 2018, Revised 27 September 2018, Accepted 16 December 2018

ABSTRACT

In this research, the recycled silicon (R_{Si}) nanopowder of 50 nm diameter was used to fabricate Silicon Microwires (SiMWs) arrays using the Cold Spraying Technique (CST). In addition, Silicon Thin Films (SiTFs) of 2μm thickness was deposited using the Thermal Evaporation Technique (TET). The fabricated SiMWs arrays with the length of 0.15-0.6μ0m and of width 0.1-0.15μm were arranged as arrays on a glass substrate, after the deposition of the initial silicon sub-layer with a thickness of 50A˚, as templates by thermal evaporation. Annealing in vacuum at 400C° was done for both SiMWs and SiTFs. In the CST process, the certified base angles were 0°, 30°, and 45°. Diagnostic and optical properties tests of these SiMWs and SiTFs were conducted. The results show that the deposited wires are crystalline with a direction of 111, and by increasing the deposition angle, the transmittance reduces and the absorbance increases due to internal reflections among extended SiMWs. The initial annealing of the substrate help in the increasing value of the transmittance when it is compared with the normal thin film, which shows more absorbency, making the fine wire applicable for solar cells and other optical applications. Consequently, the optical transparency of the SiMWs will be adequate to figure out their alignment.

Keyword: Cold Spraying, Microwire, Transmittance, Deposition Angle, Internal Reflections.

1. INTRODUCTION

Silicon Microwires (SiMWs) arrays are gaining a lot of interest because it is a highly efficient material for many applications. A micro-nano technology is able to utilize artificial means for the treatment of materials related within the size category of micro-nano meters. In the 1960s, the arrangement of a large number of microscopic transistors on a single chip help established microelectronic circuits, which improved the performance, functionality, and reliability of electronic devices. The advancement in the microelectronic circuits led to the development of electronics products such as personal computers, laptops, tablets, and mobile phones [1]. Recently, microparticles and nanoparticles draw considerable attention due to their small size. These particles find their applications in the field of ceramics, catalysis, fuel cells, solar cells, electronics, chemical-mechanical polishing, and data storage [2].

*E-mail: *adr.alaaa@gmail.com*

Fabrication of nanowires (NWs) or microwires (MWs) for silicon or other materials can be produced by many different methods such as Chemical Vapour Deposition (CVD), cold spraying, laser ablation, thermal evaporation, solid reaction, [4], sputter deposition [5], imprint lithography, and electrodeposition [6]. Those methods usually used either bottom-up growth mechanisms or top-down etching processes [3]. The researchers noted a difference in most of the properties of microwire compared to thin films for the same materials; this fact has led to serious consideration on the devices fabrication and the manufacturing processes [7]. A group of researchers have focused on the preparation conditions effects in SiMWs. Wang *et al*. [8] used a melt extraction technique to fabricate Fe-6.5wt% Si microwires with 2~30cm in length, with a fan-like microstructure. The authors concluded that the Fe-6.5wt% Si microwires can be successfully used as cores or sensors with high frequency and low induction. Chen *et al*. [9] fabricated p-type-silicon microwire (p-Si MW) arrays with a length of 10μm ornamented with amorphous hetero-metal impurities such as molybdenum sulphide for water photoelectrolysis via photolithography and dry etching techniques. The p-Si MW was used as a photocathode material for the solar hydrogen evolution. Chen *et al*. [10] fabricated silicon nanowire arrays of 7.8μm length/WO_3 core/shell photoelectrode through the Metal-Catalyzed Electroless Etching (MCEE) process, after the dip-coating airing and annealing method were done for neutral pH water splitting applications. Halima *et al*.[11] fabricated metal-free black silicon which was prepared through Metal-assisted wet Chemical Etching (MaCE), using hydrofluoric acid HF to drive the nanostructuring. The heights of the microstructural are 6.4μm to 30.8μm depending on the etching time for solar-powered hydrogen generation applications.

Another research focused on optical and electrical properties. Hu *et al*. [12] fabricated hetero-structures made of hierarchical Si core microwires covered by SiO_2 nanowires, which were shaped as multiple junctions to the cores. These structures have been created on a large scale. It can be seen that the Si wires are single crystals with a diameter of 1-3μm, while the SiO_2 nanowires are amorphous with a diameter of 30-80 nm. The materials are expected to become important for optical fibres, low-dimensional waveguides, high-bandwidth optical signal processing devices, and scanning near-field optical microscopes. Conventionally, the SiMWs were manufactured using various techniques, as previously mentioned. In particular, the Cold Spray Technique (CST) is affordable. In CST, the type and temperature of the gas used are controlled by powder particles in the spraying process [13]. The CST includes the acceleration and impact for a range of solid particles size on a substrate to form a coating with different thicknesses.

The particles are accelerated in a supersonic gas jet which can be produced using the converging-diverging de Laval nozzle. Particles impinging on a substrate will either rebind from the substrate (with or without causing erosion), or bond with the substrate depending on the type of material and the impact of particle velocity on the substrate. It has been widely reported that many metallic, alloys and composite materials coating can be readily deposited by the cold spray [14,15]. Structural, electrical, and optical measurements of SiMWs are the properties that are mostly investigated due to their important applications [16]. It is worth mentioning that the Si wires used coating from reduced graphene oxide to enhance its photoelectrochemical properties [17]. The NWs and MWs arrays have previously been shown to have little reflective losses compared to planar semiconductors. Optical path length and minority carrier diffusion length also should have either a high absorption coefficient or a transcendent light trapping [18]. The good optical properties of SiNWs and SiMWs reduce the cost of solar power by using inexpensive substrates and a lower quantity and quality of the semiconductor material [19]. Silicon nanowires SiNWs, known as nanowhiskers, have gained much attention due to their nonpareil physical properties and possible applications in the fields of nanoelectronics, nano optoelectronics and nano photovoltaics [20].

Wire solar cells fabrications include using even crystalline or amorphous silicon. Other methods of growth techniques include vapour-liquid-solid (VLS) growth, metal-catalysed chemical etching, molecular beam epitaxial MBE, metal–organic chemical vapour deposition, and deep reactive-ion etching [21]. SiNWs and SiMWs-based solar cells on glass substrates (which are still finite in the literature) have been fabricated by many methods, due to their promising applications, materials affluence, non-poisonous nature, and low-cost low-temperature [22]. The knowledge of recycling of the Si wafer to produce a chip or powder preparation is already in use for recycling, and the costs associated with recycling are not excessive. Fthenakis [23] studied the recycling of thin-film solar cells after manufacturing waste. The recycled materials were Tellurium (Te), Cadmium (Cd), and glass. Odo *et al*. [24] produced nanocrystalline silicon powder in the 100nm range by using a vibratory disc mill in a top-down synthesis route from single crystalline silicon wafers and a polycrystalline bulk. Cosnita *et al*. [25] focused on the sustainable recycling of end-of-life silicon photovoltaic (Si-PV) modules. The dismantling of the Si-PV modules (poly-crystalline Si-PV modules) of the Si-PV waste material was prepared by shredding, and then the scraps were milled. Zhao *et al*. [26] fabricated β-SiC by using recycled waste crystalline silicon, including waste polysilicon (photovoltaic industry), single crystal silicon (waste chip), after crushing and milling. Shin *et al*. [27] created an innovative method for the recycle process of recovering silicon (Si) wafer from solar panels. From the above works, it can be seen that an important area of research in this field is the synthesis of microwires by the cold spraying technique with different deposition angles reflected on sizes, shapes, and controlled disparities of SiMWs structural, electrical, and optical properties.

2. EXPERIMENTAL METHODS

2.1 Preparation of the Si Powder

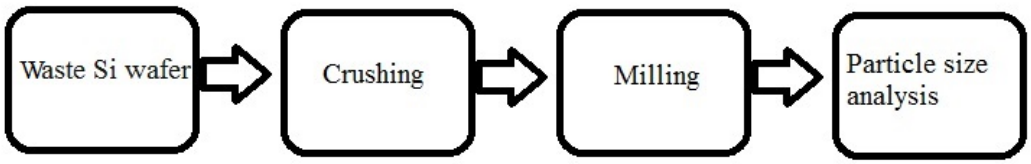

Figure 1(a). The flowchart of Si recycling steps.

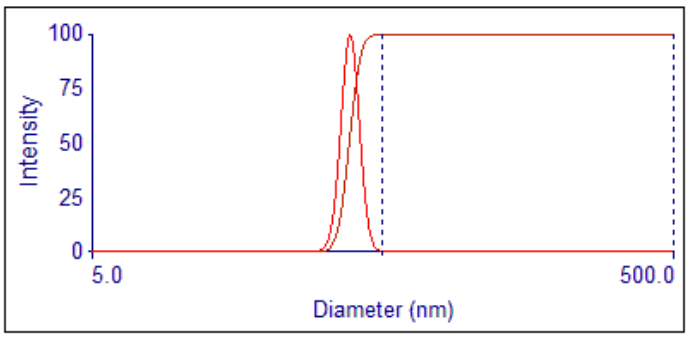

Figure 1(b). The Silicon particle size distribution.

The experimental steps to prepare Si powder are listed in Figure 1(a). The waste Si wafer was crushed to about 1μm. Then, it was milled by using 40 mill balls (CAPCO English) for 3 hours. The particle size test for powder was performed by Brookhaven Nano Brook 90 plus USA, and the size was less than 50nm, as can be seen in Figure 1(b).

2.1 Preparation of Substrates

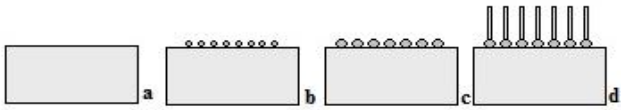

Figure 2. A schematic illustration drawing for the fabrication of SiMWs; a) substrate b) after implantation c) annealing (d) after spraying.

The growth steps were illustrated as a sketch in Figure 2 for the fabrication of the silicon microwires (SiMWs). The substrates that were used are cleaned laboratory glass slides with dimensions of 2×2×1.2cm. Preparing sub-films - a thermal vacuumed evaporation technique (TET) of type (EDWARDS) was used to fabricate a film with the thickness of 50A˚ from pure Si powder with 99.99% purity from US Research Nanomaterials, Inc. The deposition rate was 2nm/s at 10^{-4}torr. The distance from the substrate to the evaporation sources are about 12cm. Annealing was done using a vacuum furnace of type (IVOCLAR), for 30 minutes at 400°C.

2.2 Preparation of SiMWs and SiTFs

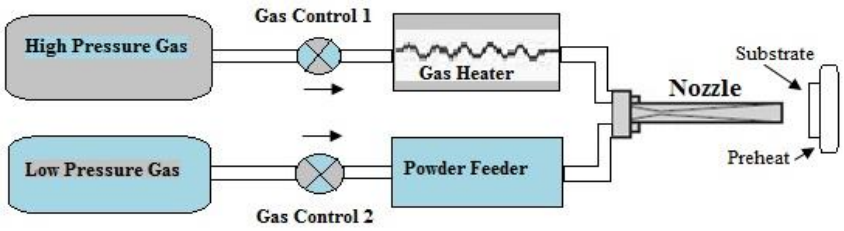

Figure 3. A schematic diagram of the cold spray system.

Preparing SiMWs from the recycled Si powder using CST: The low-velocity (gas-powder) mixture moves from the feeder into the pre-chamber. Helium gas was used as a carrier. The spray parameters are gas temperature 25ºC at a 20cm distance and 100ºC substrate temperature, gas to flow was 2.5±0.01L/min and the pressure was 7bar, as shown in Figure 3. The deposition angle likewise has been changed by changing the basis by angles of 0°, 30° and 45°. Preparing SiTFs from recycled Si powder was also done by a TET, with the same parameters mentioned above. The deposition angle has also been changed by changing the basis by angles of 0°, 30°, and 45°, and the thickness was 2μm.

2.3 Inspection

In order to study the structural properties, the nature and the crystal growth of the deposited films at different deposition conditions, X-ray Diffraction (XRD) measurements were done using Philips PW 1050 X-ray diffractometer of (1.5406 Å) from Cu-kα. In order to observe the surface topography of the deposited thin films, Atomic Force Microscopy (AFM) micrographs were taken with a digital device (AA3000, Angstrom Advanced Inc. USA). The scanning electron microscope SEM (type S-4160) study was carried out using the Electron Gun Tungsten heat filament, with a resolution of 3 nm at 30kV and an accelerating voltage of 200V to 30kV. The double–beam UV-VIS optical test was done by using (CECIL7200) spectrophotometer where the measurements were done from 300-900nm. The optical test measures the transmittance of the fabricated films and micro-wires. The electrical resistivity was measured directly using an electric prob.

3. RESULTS AND DISCUSSION

3.1 SEM of Sub-layer Results

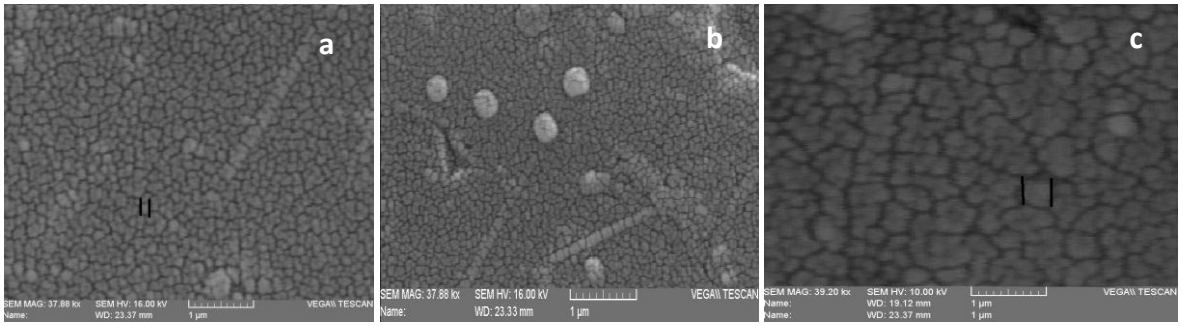

Figure 4. SEM of Si sub-layer after annealing with different substrate angles; a = 0˚, b = 30˚, and c = 45˚.

Figure 4 illustrates the SEM images of the deposited Si sub-layer film surface on the glass substrate after annealing. The growth of close grains of about 0.1-0.2μm to 0.3-0.4μm can be seen at the top surface of the glass. The substrate angle of 0˚ in (a) was adopted as the foundation intended for SiMWs and SiTFs growth later; this was stressed by Pan *et al*. [28].

3.2 X-Ray Diffraction Analysis

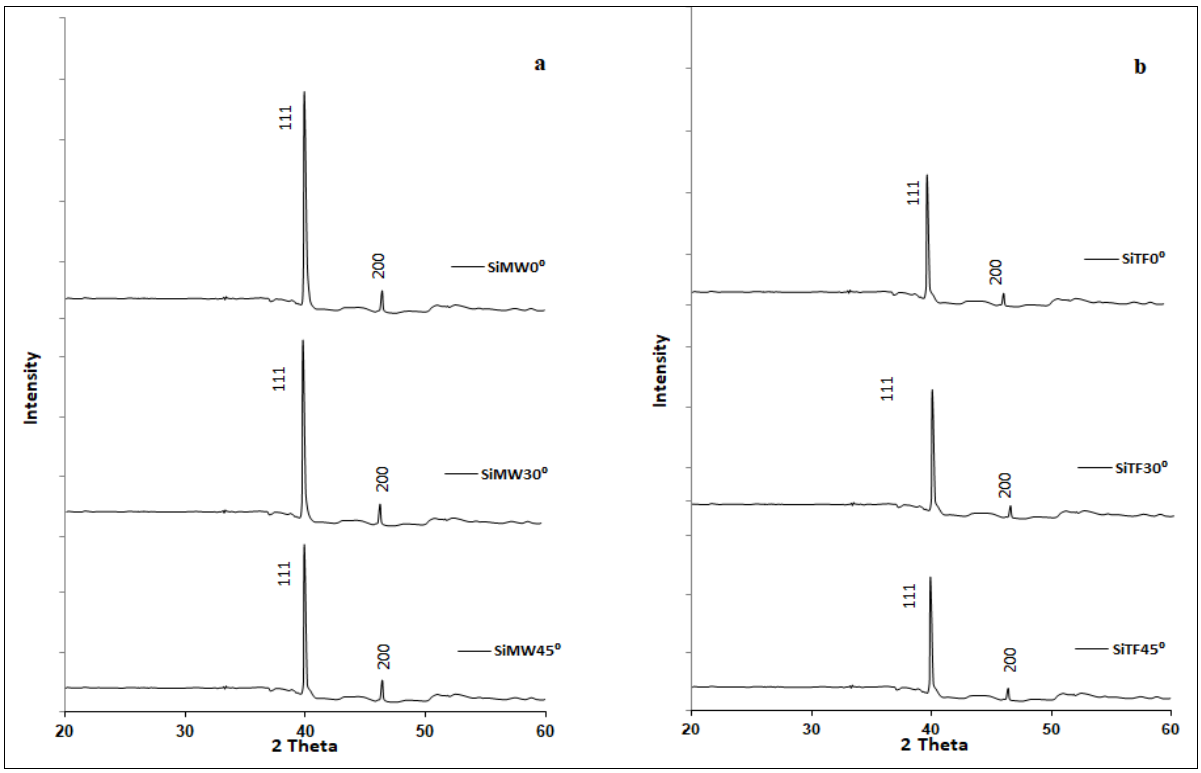

Figure 5. XRD spectrum of films at different substrate angles; (a) SiMWs, and (b) SiTFs.

Figure 5 shows the XRD results of SiMWs and SiTFs, where Figure 5 (a), (b) and (c) are for SiMWs and Figure 5 (d), (e) and (f) are for SiTFs. It was found that SiMWs and SiTFs were crystalline and that SiMWs shows higher intensity peak. The diffractograms were recorded in the 2θ range where the most intense reflexes of Si peaks are at 39.893° and 46.384°. The most

prominent peak was found at 39.89° due to the preferred orientation [29, 9] corresponding to the Si (111) emphasis cube crystallized as stated by the Joint Committee on Powder Diffraction Standards JCPDS 35-1158. No peaks appear for other component, consequently, a metal of Si 100% was deposited.

The scope of investigation of XRD to SiMWs and SiTFs has not been widely considered in the literature, a study by Gonzalez *et al*. [29] is probably the only work. To determine the a-lattice constant from the X-ray spectrum, the following formula in Eqn. (1) was used [6, 22]:

$$\frac{1}{d} = \left(\frac{h + k + l}{a} \right) \tag{1}$$

where *d* is the Lattice Plane Spacings (distance between adjacent planes), *h*, *k*, and *l* are Miller-indices, and *a* is the Lattice Parameter (standard lattice parameter for Si a_{ST} = 3.903). Table 1 shows the structural result of SiMWs and SiTFs. Lattice parameter for the SiMWs and the SiTFs were slightly changed with deposition angle. The preferred plane (hkl) in polycrystalline coat, in which there is maximal growth (preferred orientation), can be described by the texture coefficient in Eqn. (2):

$$T_{c(hkl)} = \left(\frac{I_{m(hkl)} / I_{ASTM(hkl)}}{(\frac{1}{M}) \sum \frac{I_{m(hkl)}}{I_{ASTM(hkl)}}} \right) \tag{2}$$

where $T_{C\,(hkl)}$ is the texture coefficient of the (hkl) plane, $I_{m(hkl)}$ is the measured intensity, $I_{ASTM(hkl)}$ is the American Standard for Testing Materials (ASTM) which is the intensity standard of the corresponding powder, and *M* is the number of reflections observed in the X-ray diffraction trace. As shown in Table 1, $T_{C\,(hkl)}$ changes with SiMWs only.

Table 1 Structural result of SiMWs and Si SiTFs

	SiMWs0°	**SiMWs30°**	**SiMWs45°**	**SiTFs0°**	**SiTFs30°**	**SiTFs45°**
a (nm)	3.900	3.901	3.901	3.902	3.902	3.904
$T_{C\,(hkl)}$	0.951	0.801	0.800	0.902	0.800	0.801
C_S (nm)	67	81	109	89	90	91

The average crystallite size (C_S) of the SiMWs and the SiTFs were estimated using the Scherrer's formula [13], and the results were shown in Table 1. Crystallite size increased as deposition angle increased, due to the augmentation in the deposition rate.

$$C_S = \left(\frac{0.94\lambda}{\Delta_{(2\theta)} \cos\theta} \right) \tag{3}$$

where:

λ is the x-ray wavelength (Å),
$\Delta_{2\theta}$ is the Full Width at Half Maximum (FWHM) (in radian)
θ is the Bragg diffraction angle of the XRD peak (in degree)

3.3 SEM of Films Results

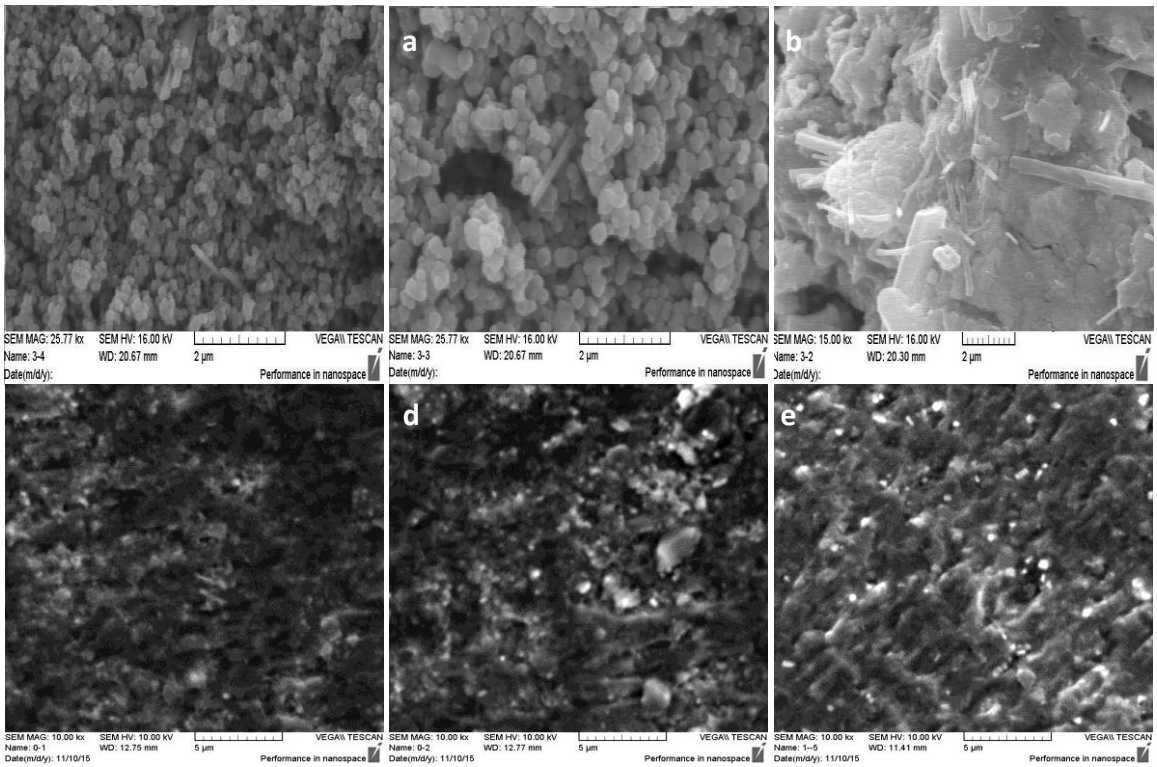

Figure 6. (SEM) top view micrograph image for SiMWs and SiTFs grown on different substrate angles; (a, d) =0˚, (b, e) =30˚ and (c, f) =45˚.

Figure 6 shows the SEM images of the top view upper surface of SiMWs and SiTFs, The effect of deposition angles on the growth direction of the SiMWs and SiTFs can be observed in Figure 6(a, b and c) and Figure 6 (d, e and f) respectively. The growth direction is the direction preferred by the developing Si wires, hence, affecting the direction of these wires and subsequently affecting the applications. Moreover, in Figure 6 (a), it was found that compact wires are aligned in 1-D perpendicular to the direction of the base and it is the perfect state, while (b) and (c) represent angles of 30˚ and 45˚ respectively. In Figure 6 (b), the wires are thicker and are shorter compared to wires in Figure 6 (a). Whereas there is a semi-regular shape in Figure 6 (c) and random, and tangled shape of wires in Figure 6 (d). Hence, changing the deposition angle affects the growth of the wires on the base, where the deposition process have more kinetic energy instead of thermal, enabling them to arrange their growth towards the vertical axis with vertical-alignment during plastic deformation [30].

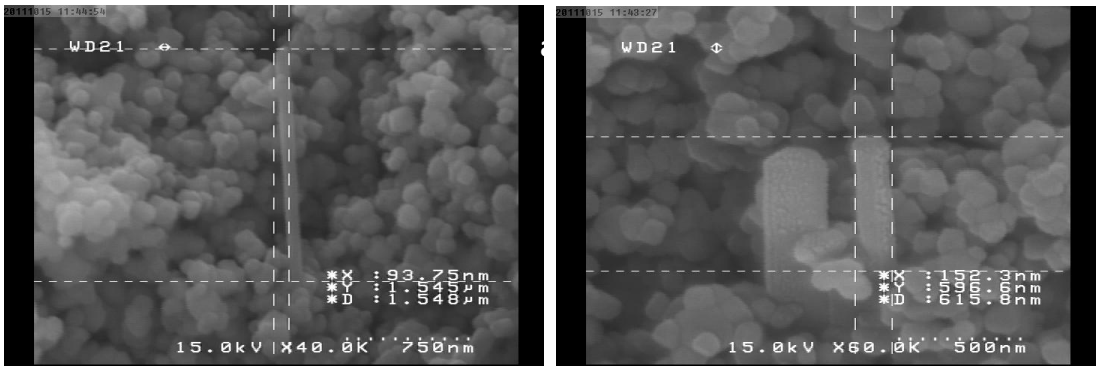

Figure 7. (SEM) A micrograph image for SiMWs at different substrate angles where (a) at 0˚ and (b) at 30˚.

Figure 7 (a) represents the surface of the rod-like shaped of Si assembly deposited wires and precipitated 0˚ angle for a substrate with 0.1μm cross-section and more than 1.54μm length. While in Figure 7 (b), it is a 30˚ angle for a substrate with 0.15μm cross-section and about 0.6μm length.

3.4 Atomic Force Microscopy Analysis

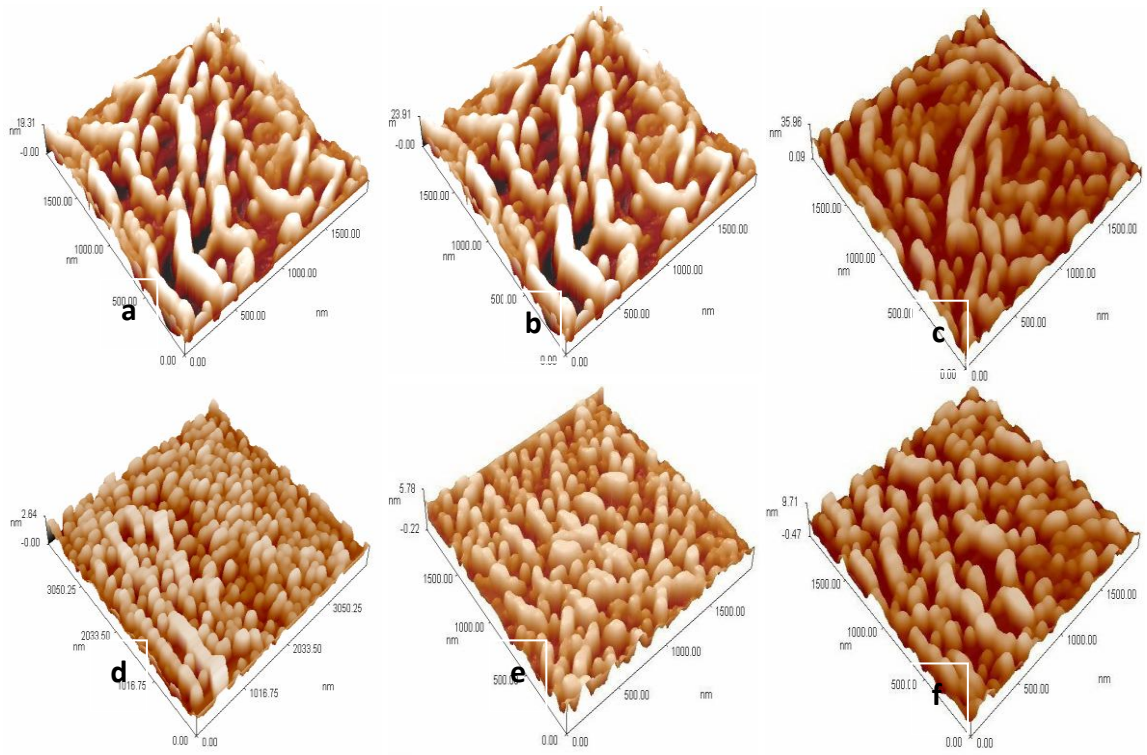

Figure 8. 3D AFM results for different angles for SiMWs (a, b, c) and SiTFs (d, e, f).

The AFM results are shown in Figure 8. In particular Figure 8 (a), (b) and (c) are for SiMWs at substrate angles of a = 0˚, b = 30˚ and c = 45˚, respectively. Whereas, Figure 8 (d), (e) and (f) are for SiTFs at substrate angles of a = 0˚, b = 30˚ and c = 45˚, respectively. SiTFs have almost perfect smooth layer surface of the deposited samples, while SiMWs is rougher because of the influence of the vertical-alignment of SiMWs compared to SiTFs at the same thickness [32]. Table 2 shows the roughness parameters of SiMWs and SiTFs.

Table 2 Roughness parameters of SiMWs and SiTFs

Parameter (nm)	SiMWs0°	SiMWs30°	SiMWs45°	SiTFs0°	SiTFs30°	SiTFs45°
Roughness	19.31	23.91	35.96	2.64	5.78	9.71
Average Diameter	99.77	106.11	122.81	74.83	88.92	93.71

3.5 Optical Transparency

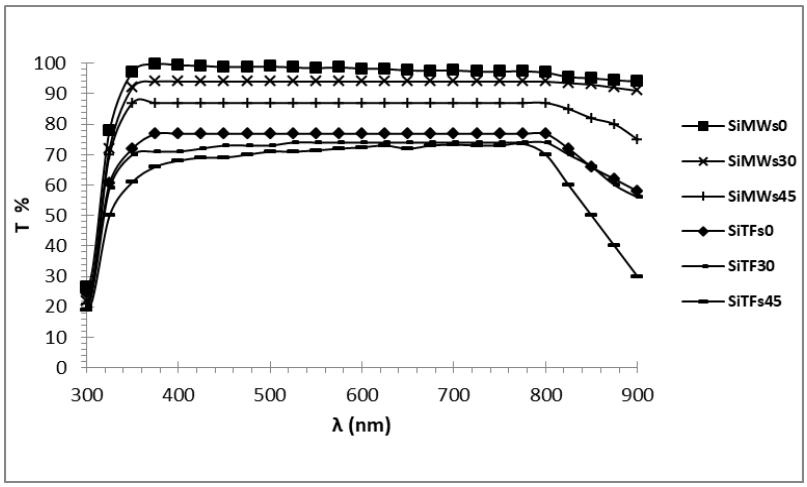

Figure 9. UV-VIS transmission spectra of SiMWs and SiTFs.

Figure 9 shows the optical transmission spectra results of SiMWs with about 2μm length and the SiTFs with 2μm thickness. Figure 9 shows a high transmittance of the SiMWs compared to the SiTFs. Improved transmittance eventuates for SiMWs, making them an anti-reflective system due to high transmission (T), and the total optical absorption (A) and reflection (R) will be low according to R + T + A = 1 [31]. SiMWs exhibited an average transmission of ~90% for the entire spectral range of 300-900nm, whilst SiTFs have an average transmission of ~70% only due to continues structure form [33] and metal nanostructures formed on a back reflector, which can couple the incident light into the surface plasmon polariton (SPP) modes in which electromagnetic excitations coupled to electron oscillations propagate along the metal-dielectric interface, resulting in sub-wavelength optical confinement.

With the increasing deposition angle of the substrate, the length of the wire was reduced as shown in SEM and the surface roughness results were increased. This increment will reduce the penetration and increase the reflection. Therefore, they have a crucial role in increasing the amount of irradiation transmittance. Also, the particle sizes of the films and wires have a clear effect, as shown in Table 1. The increase in granular size has a negative effect since it is the SiMWs for 67nm to a 109nm elevation of about 60% and a slight difference in SiTFs for 89nm to 91nm only.

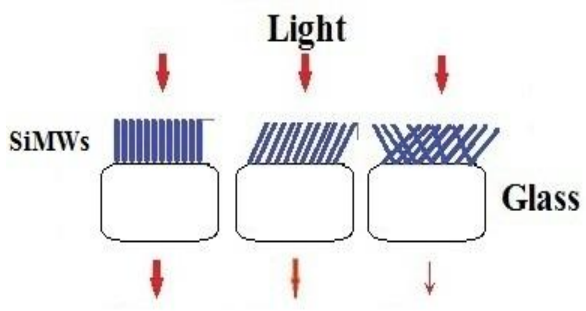

Figure 10. A diagram which shows the light spectra falling on SiMWs deposited at different angles.

Figure 10 shows a diagram of the interaction mechanism of the incident light on the SiMWs and the transmitted light with microwire alignment, the intensity of the cross decreases with the increase in the angle of deposition, which means that there is low access of light beam. It can be realized that uniform SiMWs with low surface roughness force light to pass as shown in Figure

10, micro losses arise from small-scale alignment distortion of SiMWs. The effect of particle sizes of the silicon in the results of XRD, SEM and the AFM for assembled silicon shows a direct proportion to the increase in size and increase in roughness and pre-annealing, which propagates uniformity structure, as shown in Figure 5, 6, and 8.

3.6 Electrical Resistivity

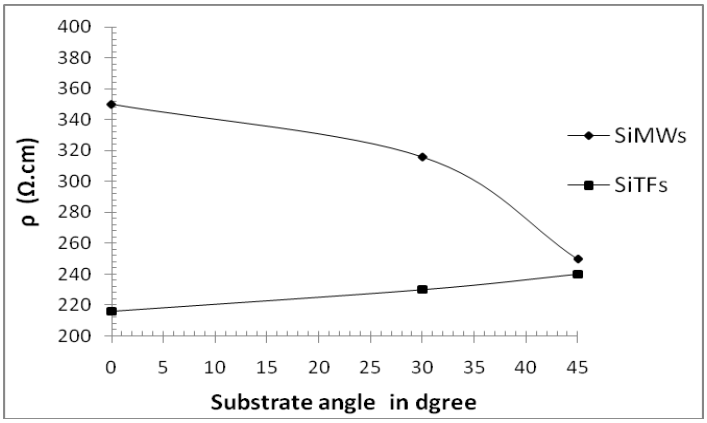

Figure 11. The electrical resistivity of SiMWs and SiTFs with the substrate angle.

Anisotropy of the resistivity increases with the directions of the SiMWs. Figure 11 plots SiMWs and SiTFs resistivities at 298Kº as a function of directions of the substrate during deposition. The resistivity of SiMWs is in the range of 350 Ω-cm to 250Ω-cm, and it decreases as the angle of the substrate increases, which may be due to the increasing cross-linking and electric contact points among the array wires when increasing the deposition angle of the substrate, as denoted in Figure 7(c). Moreover, SiMWs have a parallel connection between wires and the charge transfer impedance at the electrolyte–semiconductor interface [10].

While the resistivity of SiTFs is in the range of 216 Ω-cm to 240Ω-cm, and it slightly increases as the angle of the substrate increases. This is might be related to the non-homogeneity that takes place in SiTFs at a higher angle, where irregularity is increased as seen in the SEM image in Figure 7 (d), (e) and (f). A clear anisotropy is seen for microwire widths below 100nm, with the smallest effect in the (111) direction. The anisotropy of the resistivity becomes less pronounced with the increase of the substrate angle until it eventually disappears as the SiMWs resistivity approaches the film resistivity. The increase in the resistivity referred to the loss which may have originated from the scattering effect of the electrical conductivity caused by the discontinuities in the geometry.

4. CONCLUSIONS

This study shows that the process of recycling the waste silicon wafer from end-of-life from grinding, milling up to the production of nanoparticle (where it can be used as a product powder itself), or in the preparation of films or other devices using suitable techniques can be achieved. The simple cold spraying technique is a reliable method to fabricate SiMWs from the recycled Si nanopowder, the Si thin films can be grown after choosing the suitable deposition direction and the thermal evaporation technique. The SiMWs were of 0.1-0.15μm diameter and 0.6-1.54μm length. Long SiMWs can provide more compatible material structure and fabrication procedures in applications to fabricate optoelectronic devices. Low transmittance indicates the reduction of the alignment of micro-silicon wires. Therefore, it is only suitable at the absorption but not appropriate as a visual window. This knowledge may help improve the SiMWs that were

utilized as an anti-reflection layer caddying by Si sub-layer through vertical-alignment and high transparency.

REFERENCES

[1] G. A. Mansoori & T. F. Soelaiman, "Nanotechnology–An Introduction for the Standards Community", Journal of ASTM International **2** (2005**)** 1-21.
[2] J. Mittal, A. Batra, A. Singh and M.M. Sharma," Phytofabrication of nanoparticles through plant as nanofactories", Adv. Nat. Sci. Nanosci. Nanotechnol. **5** (2014)1-10.
[3] B. Hoffmann, V. Sivakov, S.W. Schmitt, M.Y. Bashouti, M. Latzel, J. Dluhos, J. Jiruse & S. Christiansen, "Wet – Chemically Etched Silicon Nanowire Solar Cells: Fabrication and Advanced Characterization", Nanowires - Recent Advances, London, INTECH, (2012) 211–230.
[4] H. Suzuki, H. Araki, M. Tosa & T. Noda, "Formation of silicon nanowires by CVD using gold catalysts at low temperatures", Mater. Trans. **48** (2007) 2202-2206.
[5] M. R. Shaner, S. Hu, K. Sun & N. S. Lewis, "Stabilization of Si microwire arrays for solar-driven H_2O oxidation to O_2(g) in 1.0 M KOH(aq) using conformal coatings of amorphous TiO_2", Energy. Environ. Sci. **8** (2015) 203-207.
[6] H. A. Audesirk, E. L. Warren, J. Ku & N.S. Lewis, "Ordered silicon microwire arrays grown from substrates patterned using imprint lithography and electrodeposition", ACS Appl. Mater. Interfaces. **7** (2015) 1396-1400.
[7] A. K. Palai, J. Lee, T. J. Shin, A. Kumar, S. U. Park & S. Pyo, "Solution-grown single-crystalline microwires of a molecular semiconductor with improved charge transport properties", Chem. Commun. **50** (2014) 8845-8848.
[8] S. Wang, Y. Liang, F. Ye, G. Geng & J. Lin, "Microstructure, mechanical and magnetic properties of melt extracted Fe-6.5 wt.%Si microwires", J. Mater. Process. Tech. **249** (2017) 325-330.
[9] C. J. Chen, K. C. Yang, C.W. Liu, Y. R. Lu, C. L. Dong, D. H. Wei, S. F. Hu & R. S. Liu," Silicon Microwire Arrays Decorated with Amorphous Heterometal-doped Molybdenum Sulfide for Water Photoelectrolysis" Nano Energy **32** (2017) 422-432.
[10] Z. Chen, M. Ning, G. Ma, Q. Meng, Y. Zhang, J. Gao, M. Jin, Z. Chen, M. Yuan, X. Wang, J. Liu & G. Zhou, "Effective silicon nanowire arrays/WO_3 core/shell photoelectrode for neutral pH water splitting", Nanotechnology **28** (2017) 1-24.
[11] A. F. Halima, X. Zhang & D. R. MacFarlane, "Metal-Free Black Silicon for Solar-powered Hydrogen Generation", Electrochim. Acta. **235** (2017) 453-462.
[12] J. Hu, Y. Bando, J. Zhan, X. Yuan, T. Sekiguchi & D. Golberg, "Self-assembly of SiO_2 nanowires and Si microwires into hierarchical heterostructures on a large scale", Adv. Mater. **17** (2005) 971–975.
[13] T. P. Singh, "Investigation of Flow Parameters for Titanium Cold Spraying using CFD Simulation", MSc thesis, The University of Waikato, New Zealand, (2010).
[14] S. R. Bakshi, D. Wang, T. Price, D. Zhang, A. K. Keshri, Y. Chen, D. Graham McCartney, P. H. Shipway & A. Agarwal, "Microstructure and wear properties of aluminum/aluminum–silicon composite coatings prepared by cold spraying", Surf. Coat. Tech. **204** (2009) 503–510.
[15] W.Y. Li, C. Zhang, X. P. Guo, G. Zhang, H. L. Liao & C. Coddet, "Deposition characteristics of Al–12Si alloy coating fabricated by cold spraying with relatively large powder particles," Appl. Surf. Sci. **253** (2007) 7124-7130.
[16] M. D. Kelzenberg, D. B. Turner-Evans, M. C. Putnam, S. W. Boettcher, R. M. Briggs, J. Y. Baek, N. S. Lewis & H. A. Atwater," High-performance Si microwire photovoltaics", Energy. Environ. Sci. **4** (2011) 866-871.

[17] Z. Huang, P. Zhong, C. Wang, X. Zhang & C. Zhang, "Silicon Nanowires/Reduced Graphene Oxide Composites for Enhanced Photoelectrochemical Properties," ACS Appl. Mater. Inter. **5** (2013) 1961-1966.
[18] E. Garnett & P. Yang, "Light Trapping in Silicon Nanowire Solar Cells", Nano. Lett. **10** (2010) 1082-1087.
[19] C. M. Lieber & Z. L. Wang, "Functional Nanowires," MRS Bull. **32** (2007) 99-108.
[20] X. Duan, Y. Huang, R. Agarwal & C. M. Lieber, "Single-nanowire electrically driven lasers," Nature **421** (2003) 241-245.
[21] M. C. Putnam, S. W. Boettcher, M. D. Kelzenberg, D. B. Turner-Evans, J. M. Spurgeon, E. L. Warren, R. M. Briggs, N. S. Lewis & H. A. Atwater, "Si microwire-array solar cells", Energy. Environ. Sci. **3** (2010) 1037-1041.
[22] V. Sivakov, G.Andra, A. Gawlik, A. Berger, J. Plentz, F. Falk & S.H. Christiansen, "Silicon Nanowire-Based Solar Cells on Glass: Synthesis, Optical Properties, and Cell Parameters", Nano. Lett. **9** (2009) 1549-1554.
[23] V. M. Fthenakis, "End-of-life management and recycling of PV modules", Energy Policy **28** (2000) 1051-1058.
[24] E. A. Odo, D. T. Britton, G. G. Gonfa & M. Harting, "Mechanism of DC conduction in silicon nanoparticles network", The African Review of Physics **7** (2012) 45-56.
[25] M. Cosnita, C. Cazan, A. Duta & I. Visa, "Recycling Silicon-PV Modules in Composites with PVC, HDPE and Rubber Wastes", Springer Proceedings in Energy, (2017) 375-394.
[26] M. Zhao, M. Johnson, W. He, G. Li, C. Zhao, J. Huang & H. Zhu, "Transformation of waste crystalline silicon into submicro β-SiC by multimode microwave sintering with low carbon emissions," Powder Technol. **322** (2017) 290–295.
[27] J. Shina, J. Park & N. Park, "A method to recycle silicon wafer from end-of-life photovoltaic module and solar panels by using recycled silicon wafers", Sol. Energy. Mat. Sol. C **162** (2017) 1-6.
[28] Z. W. Pan, Z. R. Dai, L. Xu, S. T. Lee & Z. L. Wang," Temperature-Controlled Growth of Silicon-Based Nanostructures by Thermal Evaporation of SiO Powders", J. Phys. Chem. B **105** (2001) 2507-2514.
[29] E. Quiroga-Gonzalez, J. Carstensen & H. Foll, "Structural and Electrochemical Investigation during the First Charging Cycles of Silicon Microwire Array Anodes for High Capacity Lithium Ion Batteries", Materials **6** (2013) 626-636.
[30] A. Moridi, S. M. Hassani-Gangaraj, M. Guagliano & M. Dao, "Cold spray coating: review of material systems and future perspectives", Surf. Eng. **30** (2014) 369-395.
[31] Y. J. Hung, S. L. Lee, K. C. Wu, Y. Tai & Y.T. Pan, "Antireflective silicon surface with vertical aligned silicon nanowires realized by simple wet chemical etching processes", Opt. Express. **19** (2011) 15792-15802.
[32] S. D. Jiang, T. Eggers, O. Thiabgoh, D.W. Xing, W. D. Fei, H. X. Shen, J. S. Liu, J. R. Zhang, W. B. Fang, J. F. Sun, H. Srikanth & M. H. Phan, "Relating surface roughness and magnetic domain structure to giant magneto-impedance of Co-rich melt-extracted microwires", Sci. Rep-UK **7** (2017) 1-8.
[33] K. T. Park, Z. Guo, H. D. Um, J. Y. Jung, J. M. Yang, S. K. Lim, Y. S. Kim & J.H. Lee1, "Optical properties of Si microwires combined with nanoneedles for flexible thin film photovoltaics," Opt Express **19** (2011) A41-A50.